# The Effect of Two-Way Shape Memory on the Healing of Poly (Ethylene-Co-Methacrylic Acid) and Polybutadiene Blend

EMMANUEL IGBOKWE<sup>1</sup>, SAMUEL IBEKWE<sup>1</sup>, PATRICK MENSAH<sup>1</sup>, GUOGIANG LI<sup>2</sup> and CHINMEN DAVID<sup>1</sup>

### **ABSTRACT**

Development in self-healing materials and smart composites has continuously improved for many decades and has given rise to many real-life applications with implications for engineering materials, structures, and human beings who rely on these technological innovations to further human endeavor. This study involves the use of intrinsic self-healing ability of poly (ethylene-co-methacrylic acid) thermoplastic, known by its commercial name as Surlyn 9520©, and combined two-way shape memory effect with Di cumyl-peroxide (DCP) cross-linked polybutadiene elastomer to achieve crack narrowing and closure with subsequent healing of the polymer blend surface.

The simple batch mixing process resulted in an immiscible yet compatible blend, determined by two distinct melting peaks from DSC characterization and FTIR spectroscopy analysis.

Different blends ratios of 80/20, 70/30, 60/40, 50/50 were investigated and characterized. However, the 80/20 blend was chosen to demonstrate the significance of the two-way shape memory effect, where a material experiences elongation upon cooling and contraction upon heating to achieve crack closure and effectual healing. Two sets of samples were studied; control Sample known as 2A and 2B samples were one time programmed to about 300% strain. Self-healing, which is a function of the poly(ethylene-co-methacrylic) acid component of the blend, was established for both sets of specimens. The flexural properties from three-point bending test indicate that although both sets of samples achieved good healing efficiencies, the 2B programmed samples displayed better healing efficiencies than the control by 30%.

Keywords: Shape memory Polymers, Composite, programmed samples, poly(ethylene-co-methacrylic) Acid. Self-healing, DSC Characterization, FTIR analysis.

Address: 801 Harding Blvd. Baton Rouge LA, 70815<sup>1</sup>; 114 West David Boyd Baton Rouge LA, 70803<sup>2</sup>

## 1.0 INTRODUCTION

Over the past many decades, engineers and scientists have sought to improve machines and components' service life through research and innovation. One way of achieving this is through the study of self-healing composite materials [1]. Catastrophic failures and impaired performance or functionality of structures, machines, and parts can have immense cost implications, which might transcend financial cost and human life. On 28 January 1986, the seven [2] crew members onboard the OV-099 Space Shuttle Challenger built by the National Aeronautics and Space Administration (NASA) experienced such catastrophic failures. The fatal disaster sent shockwaves across the heart of Americans and the world over. This catastrophe was attributed to the failure in a small component of the space vessel called O-rings [3]. These rubber materials are employed to seal joints along with their propulsion system. This tragedy happened when a significant drop in the environment's temperature caused the component to behave in a glassy and brittle manner, which affected their functionality. The Challenger example calls to mind that even the smallest part of an engineering system can have a tremendous impact. The key to achieving intrinsic self-healing of polymer composites lies in the material's ability to rejoin its separated surfaces and react to fill the gaps created by cracks or other forms of damage that can occur. Therefore, while this intrinsic strategy of healing composite materials works very well for small-scale damage, it can be a little more challenging where the damage is enormous.[4] During these damages, the space between failed surfaces becomes more. The surfaces need to be in contact for healing to take place. This process requires the matrix to move locally when adequately stimulated to bring the said surfaces back together and initiate the healing process [5]]. This stimulation could result from temperature, electric current, water or moisture exposure, and photo initiation. Many methods, studied over decades of research into intrinsic self-healing components, also include the close-then-heal process. This twostep healing scheme allows surfaces to be brought together for molecular entanglement of the composite materials to seal the crack [6] and mimics the healing of a wound on the skin. Some of the ways to achieve crack closure for intrinsic self-healing in polymer composites include the use of shape memory alloys [7], polymeric, artificial muscles, shape-memory fibers [8], and shape memory polymer materials. Shape memory polymers are a class of polymer materials that can note original shapes [9]. When deformed under an applied force's action, they can return to that original position under the induction of externally applied stimulus, like heating the material. Shape memory polymers provide certain advantages, making them fascinating materials to study, such as performing complex movements, ease of manufacturing, and low density [10]. Several materials possess shape memory abilities; ionomers and elastomers are two of such materials. The two-way shape memory effect is an imbued property of a material. It causes the material to attain two different shapes or configurations at different temperatures, during cooling and when heated. This phenomenon inverts most materials' natural physics, where they contract when cooled and expand when heated. SurlynTM Ionomers describe copolymers of ethylene and methacrylic acid, which have a small number of ionic groups along their backbone. They are olefin-based block copolymers with short ionic blocks, which cause attraction to each other [11]. Under the application of heat, bonds tend to reform, which forms the basis for its use as a selfhealing material. Properties like oil and grease resistance, good toughness, clarity, and low-sealing temperature make them quite suitable for several applications, found across products like golf balls, film packaging, and formula one cars.

Polybutadiene is an organic compound that contains two carbon-carbon double bonds and classified as an alkene in terms of functional groups. An alkene is any compound with at least one carbon-carbon double bond with the high cis form having high elasticity while the high Transform presents as plastic crystals [12]

One fundamental difference between one-way shape memory polymers and two-way shape memory polymers lies in their switching behavior upon actuation. In the case of one-way shape memory polymers, the material automatically reverts to its permanent shape upon exposure to some external stimuli, which remains unchanged as the external stimulus is removed. However, when it comes to two-way shape memory polymers, when two opposite incentives are applied to the material, it can switch between two states and change its shape to correspond to each one [13]. More so, in one-way shape memory, the material needs to be reprogrammed after the first cycle. Still, the switching between shapes can be achieved without reprogramming every time [14] when it comes to two-way shape memory polymers. Once the polymer is reheated above the multiphase network's switching temperature, which is related to either the melting temperature (T<sub>m</sub>) or glass transition temperature (T<sub>g</sub>), the permanent shape is recovered due to the entropic relaxation of constrained chains. [15]

The purpose of this study is to Create a composite blend made from thermoplastic Poly (ethylene-co-methacrylate acid) and polybutadiene elastomer and test the materials properties of the blend and demonstrate healing from the two-way shape memory effect via heating Technique.

# 2.0 MATERIALS & METHODS

## 2.1.1 Materials

The elastomeric material used was Cis-poly(1-4-butadiene) (PBD) with 97% cis content, which has the commercial name Budene® 1208 from Goodyear® Chemical (Akron, OH, USA). Its reported onset glass transition temperature is -104°C. The second material was Dicumyl peroxide (DCP), 99% with a molecular weight of 270, 37 manufactured by Acros Organics<sup>TM</sup>, and available from Fisher Scientific<sup>TM</sup> https://us.vwr.com/store/ DCP was added to the PBD elastomer to achieve the two-way shape memory in PBD [41]. Finally, the third material, poly (ethelene-co-methacrylate) acid (PEMA) ionomer, obtained from DuPont TM under Surlyn 9520, was utilized as the [35] thermoplastic component of the material. PEMA has a density of 0.95 g/cm³ and a melting point of 96°C. The material Blend composition mixed ratios are 80% PEMA-20%PBD, 70% PEMA-30% PBD, 60% PEMA- 40% and 50%PEMA-50% PBD.

### 2.1.2 Fabrication & Specimen Procedures

The thermoplastic PEMA pellets and polybutadiene rubber were measured on a weight scale, corresponding to varying ratios for comparison. Dicumyl peroxide was measured to fit 3% of the polybutadiene weight estimated in each blend ratio. The blend mixer was set to a temperature of 100°C with the rotor speed of 50 rpm after the heat reached

the set point [42]. The polybutadiene rubber was cut up and placed inside the mixer, allowing it to settle for about 2 minutes before adding the Dicumyl peroxide. After two minutes, the Surlyn TM ionomer was added to the mix, and the chamber was locked down. The constituents were allowed to mix for 20 minutes, and then the chamber was opened to evacuate the product. The batch mixing product was collected from the batch mixer and cut into small bits to fit into a steel mold with compression molding using a Carver® Hydraulic Compression Molding Press at 150°C with a pressure of 4.2 metric tons, equivalent to 5.9 psi. The compression molding time for the samples was 10 minutes. After compression molding, the material was allowed to cool and removed from the mold and cut into samples using a water-jet cutter.

## 2.2 Specimen Testing

#### 2.2.1 TENSILE TESTING PROCEDURE

A Quest 150 Elite controlled Measure Test Simulate® (MTS) was used to perform tensile testing at 50mm/min strain rate, done at room temperature. Five specimens were cut for each blend ratio using a waterjet cutting machine. The specimen dimensions were measured using a digital vernier caliper, recording the width and thickness corresponding to three different points along each one's gauge length. The specimen was then loaded into the MTS® system and stretched until failure.

### 2.2.2 MATERIAL CHARACTERIZATION

An FTIR analysis on the raw samples Poly (ethylene-co-methacrylic acid) and polybutadiene and the different blends investigate and compare changes in the functional groups from the blending process. Each blend specimen was captured 15 times, and the spectra output average was obtained using Microsoft excel. After that, OriginPro® Graphing & Analysis software, version 8.5, was used to plot the graphs. The material DSC analysis was done using a Hitachi 7000X DSC machine. The specimen was first placed in an aluminum pan and heated from 30°C to 120°C held before cooling with a purging rate of Argon gas at 30mL/min to -95°C. The cooling rate was 2°C/min. After that, the sample was heated from -95°C back to 120°C. In all, three cycles of heating and cooling were conducted before the specimen was returned to 30°C to conclude the test. The first heating cycle was counted as erasing the material's thermal history so that the second heating cycle could be used for evaluation. A study of the material blend's surface morphology used a Phenom ProX Scanning Electron Microscope from Nanoscience instruments. However, before observing the fracture surfaces, the samples were first coated via gold sputtering to approximately 5nm using the Denton Sputter Coater under a vacuum chamber. The images were taken with an electron energy of 15kV and around 2600X magnification.

### 2.3 Shape Memory and Bulk Programming Testing

The one-way shape memory test for the various material blend composition ratios was conducted using a Q800 Dynamic Mechanical Analyzer from TA Instruments. A compression-molded film was cut into rectangular specimens and used to perform the shape memory test.

To test the close-then heal scheme, material from the selected 80/20 blend ratio was compression molded into a 100mm X 20mm X 15 mm mold. The rectangular specimens obtained were polished on the Leco SS1000 Grinder shown in Fig. 16(a) to reduce the thickness to fit into the MTS system's grips. After this reduced thickness was achieved, they were programmed using the MTS® Landmark 370.25 system with Flex Test<sup>TM</sup> 40 Station Manager software, version 6.0 and MTS TestSuite<sup>TM</sup> Multi-Purpose Elite software, version 4.3.1.375.

## 2.4 Self-Healing Testing

The compression molding process produced two groups of specimens used in conducting the self-healing test. Three (3) sets of 2A specimens are considered the control group because they did not undergo any programming procedure [38]. Set 2B samples were programmed as described above to an average of 350% strain over three (3) specimens. After programming, the set of 2B specimens were placed in an oven for 10m minutes, already set to 100oC, where they recovered back to their rectangular shape held before they were programmed, the recovered set of 2B samples and the non-programmed set of 2A samples were then cut within the midsection using a band saw to mimic a 1.54mm deep and 0.85 mm wide crack.

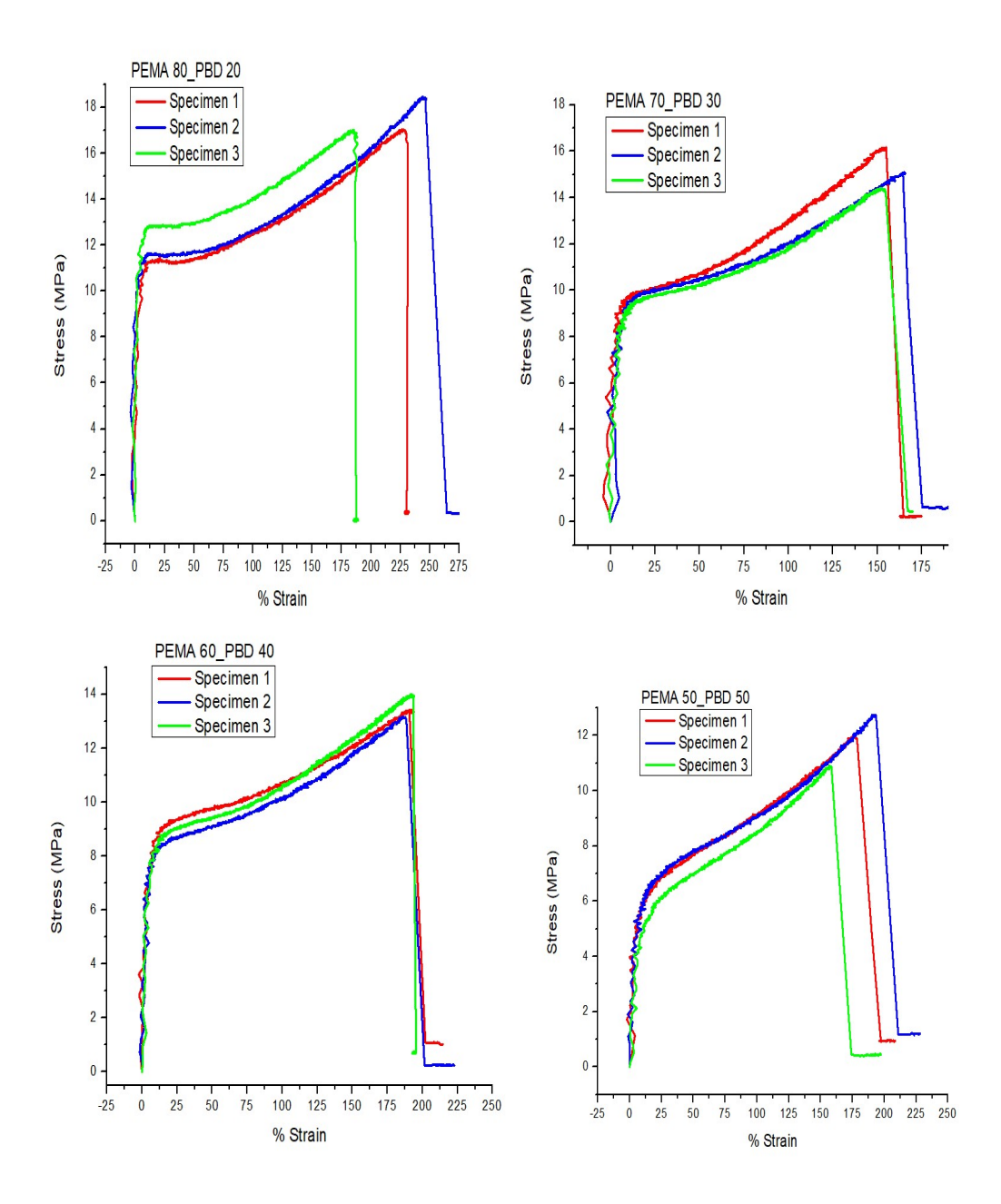
# 2.5 Determination of Flexural Properties

A three-point bending test on both Group 2A and Group 2B samples carried out to determine the flexural properties of the sample specimens using the Quest 150 Elite controlled MTS machine at a strain rate of 0.5mm/min and span length of 50mm. [40]. The flexural strain ( $\epsilon_f$ ), defined as the nominal fractional change in the length of an element of the outer surface of the test specimen at mid-span, where the maximum strain occurs, was calculated using the equation:

$$\varepsilon_{f} = \frac{6Dd}{L^{2}} \tag{1}$$
 
$$\sigma_{f} = \frac{3PL}{2bd^{2}} \tag{2}$$

# 3.0 RESULTS AND DISCUSSION

# 3.1.1 Blend Ratio Tensile Stress



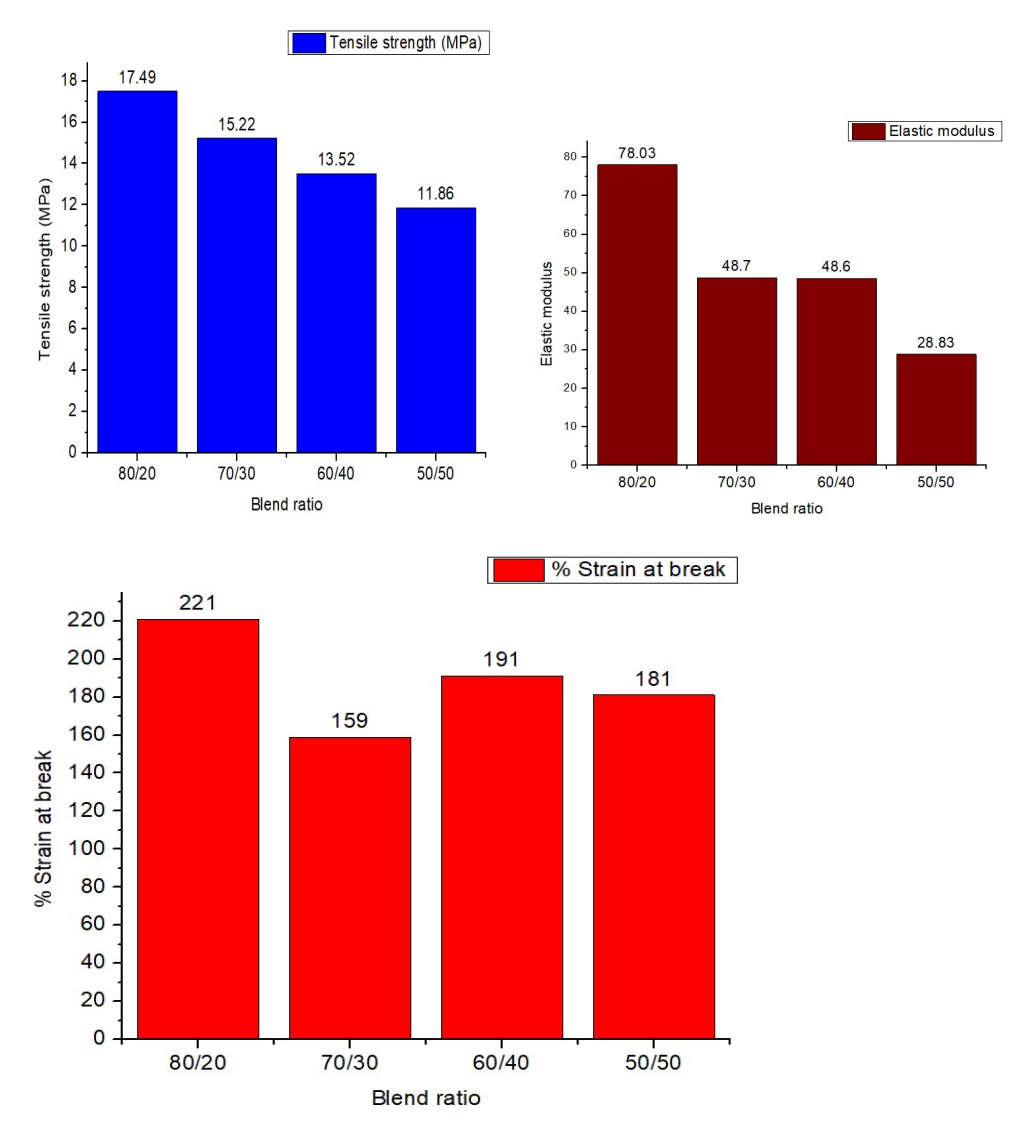


Figure 1-7. Shows the Different Bend Ratio Tensile Stress.

From the results obtained, the 80/20 blend has the highest tensile strength of 17.49 MPa, averaged over three specimens. Elongation at break of 221% was reached by the 80/20 blend before failure. The tensile strength uniformly reduces with the addition of the polybutadiene rubber phase with the 50/50 blend ratio reflecting 11.86 MPa. However, the 70/30 blend ratio achieved the least amount of average strain at 159%, even less than the 60/40 and 50/50 blends.

# 3.1.2 FTIR Analysis Result

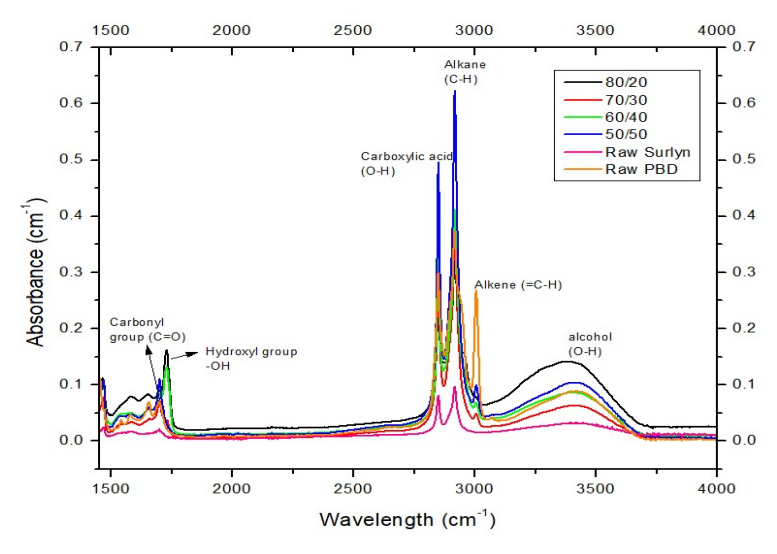


Figure 8. Shows the FTIR Analysis of Different Blend Ratio.

From the result diagram, Hydrogen bonding interaction between the carbonyl and carboxyl groups can be observed in peaks formed between them. 80/20 and 60/40 blends achieved better compatibility from the physical mixing than the other blends

# 3.1.3 One-Way and Two-Ways Shape Memory Results for all Blend Ratio

TABLE I. One-way shape memory test for Blend Ratios.

|             | 1st Cycle    |                | 2 <sup>nd</sup> Cycle |                |  |
|-------------|--------------|----------------|-----------------------|----------------|--|
| Blend ratio | Fixity ratio | Recovery ratio | Fixity ratio          | Recovery ratio |  |
|             | (%)          | (%)            | (%)                   | (%)            |  |
| 80/20       | 96.96        | 95.59          | 97.49                 | 95.93          |  |
| 70/30       | 95.97        | 88.26          | 96.2                  | 91.35          |  |
| 60/40       | 94.79        | 88.86          | 94.84                 | 92.95          |  |
| 50/50       | 89.26        | 83.29          | 89.1                  | 87.6           |  |

From the results in Table 1 above, the 80/20 blend has better shape fixity and recovery ratios than others, followed by the 60/40 ratio, which is slightly better than the 70/30 blend. These results are consistent with the TGA, SEM, and FTIR observations, which imply better interaction achieved in the 80/20 and 60/40 blends, which tend to impact their properties compared to the other two blend ratio.

TABLE II. Two-ways Shape Memory for Blend Ratios.

| Blen<br>d<br>rati<br>o | For ce (N) | Stres<br>s<br>(MP<br>a) | Program med strain (%) | CUI<br>EUO |           | CUI<br>EUC   |           | 3rd Co<br>CUH<br>EUC |              | CUI<br>EUC |           |
|------------------------|------------|-------------------------|------------------------|------------|-----------|--------------|-----------|----------------------|--------------|------------|-----------|
| 80/2<br>0              | 1.5        | 0.17                    | 155                    | 5.1<br>6   | 11.8<br>7 | 6.8<br>9     | 25.5<br>6 | 13.2<br>5            | 5.1<br>6     | 5.5<br>7   | 25.6<br>3 |
| 70/3<br>0              | 2.0        | 0.19                    | 75                     | 2.6<br>7   | 4.4       | 3.2<br>7     | 4.69      | 3.25                 | 3.3<br>9     | 3.4<br>2   | 3.69      |
| 60/4<br>0              | 5.0        | 0.35                    | 142                    | 2.6<br>3   | 6.57      | <b>4.6 0</b> | 6.52      | 4.68                 | 5.7<br>5     | N<br>A     | NA        |
| 50/5<br>0              | 5.0        | 0.32                    | 107                    | 2.1<br>2   | 3.45      | 4.7          | 4.91      | 3.4                  | <b>4.2 6</b> | N<br>A     | NA        |

In the end, it can be said that the poly (ethylene-co-methacrylic acid and polybutadiene blend was able to display a two-way shape memory effect as shown across all the combinations tested. Also, the 70/30 mixture, even though it was strained to just 70% during the programming cycle, clearly exhibits the two-way shape memory effect. The 60/40 and 50/50 blends display a two-way shape memory effect, but given the more feasibility of the 80/20 composition, this blend ratio was chosen to test the two-way mechanism for crack closure self-healing.

# 3.1.4 DSC Analysis Testing Result

TABLE III. Shows the DSC Exothermic Curve for Blend Ratios.

| Ratio<br>(PEMA/PBD) | Peak<br>(°C) | Enthalpy of Crystallization (PBd) ΔHc (mJ/mg) | Peak<br>(°C) | Enthalpy of Crystallization (PEMA) ΔH <sub>c</sub> (mJ/mg) |
|---------------------|--------------|---|--------------|--|
| 80/20               | -33.80       | -2.62   | 69.10        | -34.00   |

| 70/30 | -46.20 | -7.25  | 68.90 | -26.50 |
|-------|--------|--------|-------|--------|
| 60/40 | -43.40 | -19.00 | 64.90 | -48.10 |
| 50/50 | -40.86 | -5.39  | 68.80 | -17.7  |

TABLE IV. Shows the DSC Endothermic Curve for Blend Ratios.

| Ratio<br>(PEMA/PBD) | Peak<br>(°C) | Enthalpy of<br>Crystallization<br>(PBd)<br>ΔH <sub>c</sub> (mJ/mg) | Peak<br>(°C) | Enthalpy of<br>Crystallization<br>(PEMA)<br>ΔH <sub>c</sub> (mJ/mg) |
|---------------------|--------------|--|--------------|---|
| 80/20               | -24.9        | 5.11   | 91.60        | 15.30   |
| 70/30               | -22.90       | 5.42   | 89.60        | 15.30   |
| 60/40               | -19.30       | 14.2   | 91.20        | 25.50   |
| 50/50               | -32.33       | 2.39   | 87.71        | 18.30   |

DSC Analysis: The 80/20 blend showed a melting point at 91.6°C, and the 50/50 blend showed melting at 87.70°C, 80/20 blend two distinct crystallization temperature was 69.10°C and -33.80°C corresponding to PEMA and PBD.

# 3.2 X-ray Diffraction and TGA Analysis

From figure 9-10 below, the 80/20 blend shows the best stableness, with only 4.69% loss at 40°C. Nonetheless, it is notable that the 80/20 and 60/40 blends display less loss than the 70/30 and 50/50 blend ratios. At the end of the heating cycle, with the temperature at 550°C, results show that 70/30 and 50/50 blends lost a higher percentage of initial weight, about 98.85% and 99.35%, respectively. Conversely, the 80/20 and 60/40 ratios show only 83.35% and 82.83%, respectively. Overall, one can deduce that the 60/40 blend may have better thermal stability compared to the others. As can be observed from the XRD calculated results, the domain size in the 50/50 blend is more significant than all the other blends. Nonetheless, for the other 80/20, 70/30, and 60/40 blend ratios, crystallite size increased with the higher thermoplastic phase. The 70/30 blend was found to have the least percentage crystallinity, which may explain the drop in the poly (ethylene-co-methacrylic acid) melting peak observed during the DSC measurement.

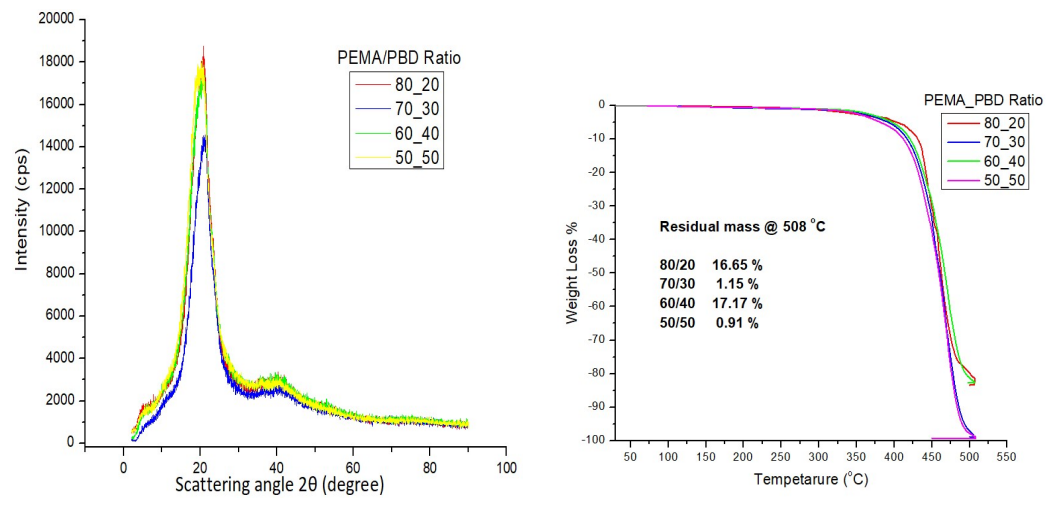


Figure 9-10. Shows the X-ray Diffraction and TGA Analysis of Blends.

# 3.3 SEM Results of Blend Ratio

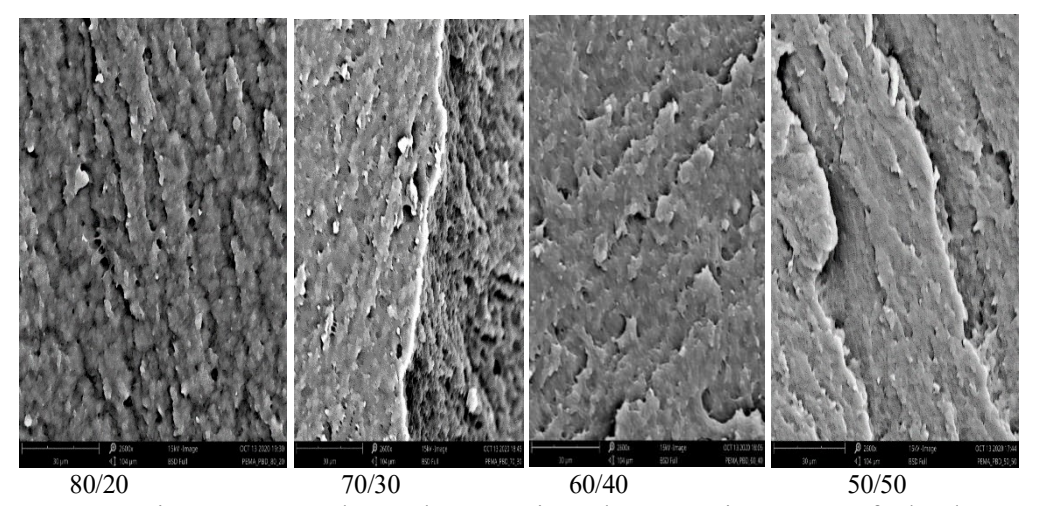


Figure 11-14. Shows the Scanning Electron Microscopy of Blends.

As shown on the spectra above, carbonyl peak appears between, shifting to the right with the 80/20 blend having the highest peak. The 60/40 blend ratio shows a broader peak, although at absorption lower than the 80/20 ratio. A broader peak may imply stronger hydrogen interaction. The 70/30 blend shows minimal peak absorbance compared to the previous two. The 50/50 blend did not show any peak within this region. It can be deduced that the 80/20 and 60/40 blends achieved better compatibility from the physical mixing than the other blends.

# 3.4 Viscoelasticity Test Analysis

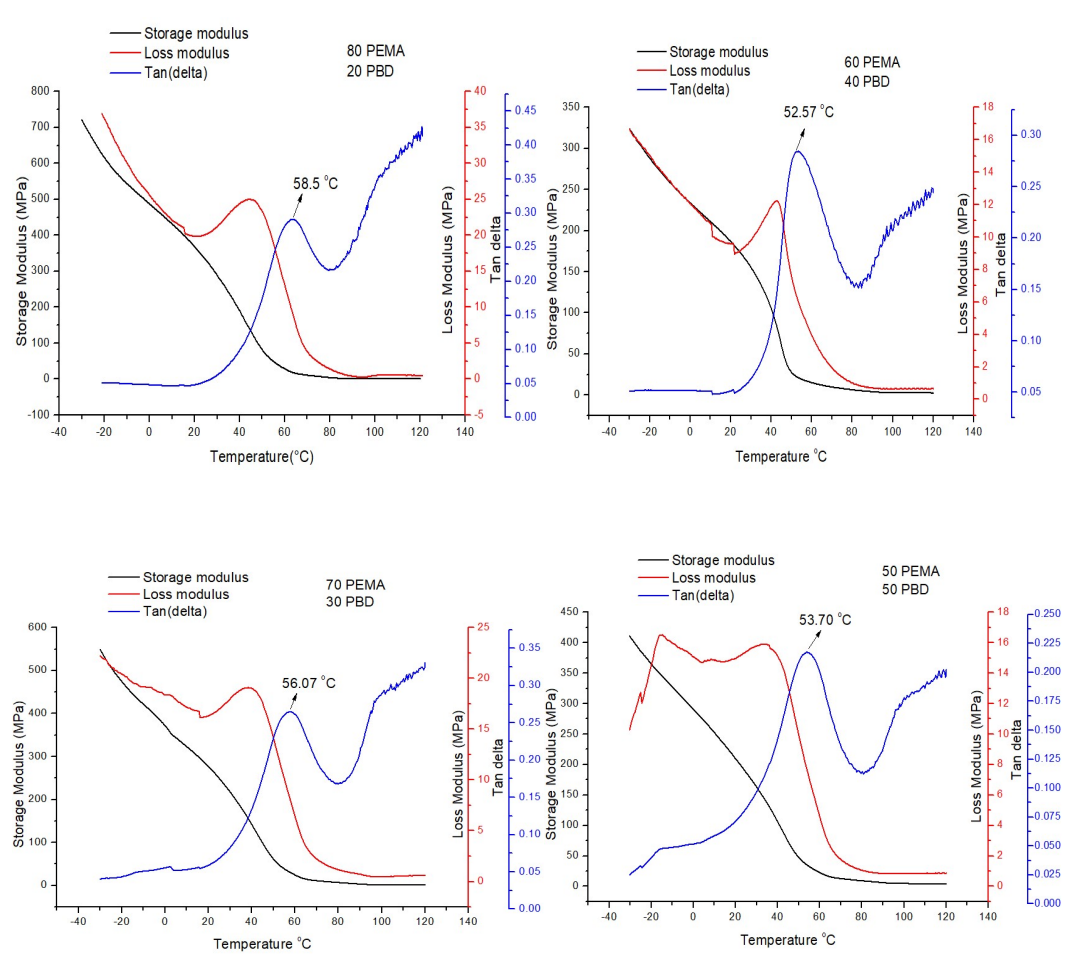


Figure 15-18. Above Shows the Viscoelasticity Test Analysis of Blends.

From the dynamic mechanical analysis (DMA) results shown in the graphs above, the polymer blends' glass transition temperatures, as represented by the tan delta peaks, reduce as the polybutadiene phase increases with the 80/20 blend ratio having the highest transition temperature of 58.8°C. However, the 50/50 blend ratio was slightly higher than the 60/40 blend. As consistently shown across all material blend ratios, as the melting point is approached at high temperature, the storage modulus drops to near zero. The once stiff material becomes rubbery.

# 3.5 Close-Then-Heal Mechanism

# 3.5.1 GROUP 2A CONTROL SAMPLES

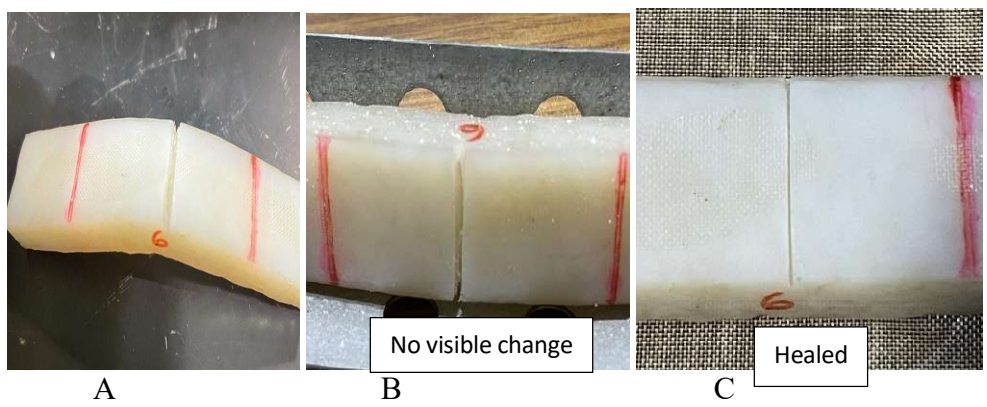


Fig. 19-21. Shows Control Group 2A loading and Healing.

# 3.5.2 GROUP 2B PROGRAMMED SAMPLES

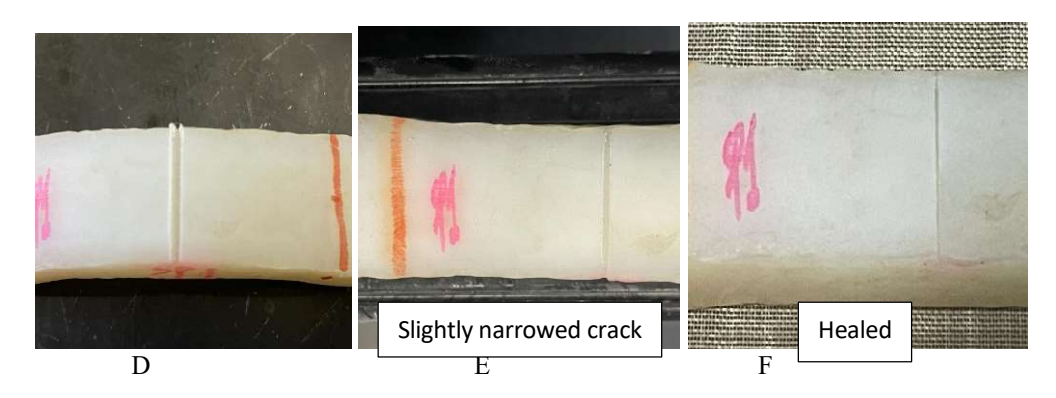


Fig. 22-24. Shows Programmed Group 2B loading and Healing.

TABLE V. Shows the Healing Efficiency of Group 2A Control Samples.

| Material Group | Healing Efficiency (%) |         |         |  |
|----------------|------------------------|---------|---------|--|
|                | Cycle 1                | Cycle 2 | Cycle 3 |  |
|                | 76.68                  | 65.67   | 44.15   |  |
| 2A             | 73.79                  | 57.52   | 43.05   |  |
|                | 89.49                  | 78.06   | 64.80   |  |
| M              | 79.99                  | 67.08   | 50.67   |  |
| SD             | 8.36                   | 10.34   | 12.25   |  |

TABLE VI. Shows the Healing Efficiency of Group 2B Programmed Samples.

| Material Group | Healing Efficiency (%) |         |         |  |  |
|----------------|------------------------|---------|---------|--|--|
|                | Cycle 1                | Cycle 2 | Cycle 1 |  |  |
|                | 96.13                  | 91.62   | 74.22   |  |  |
| 2B             | 84.71                  | 68.63   | 49.37   |  |  |
|                | 80.28                  | 54.72   | 41.45   |  |  |
| Mean           | 87.04                  | 71.66   | 55.01   |  |  |
| SD             | 8.18                   | 18.64   | 17.10   |  |  |

comparison of flexural stress: The average flexural stress of the 2A control group was higher than the 2B group for the first cycle. The programming process stretches the material, and the molecules align in the direction of the applied force. Upon recovery, however, not all the molecules are fully recovered due to molecular slippage.

The first cycle shows the control 2A samples with 79.99% and 87.04% for the programmed 2B from the healing efficiency results. By the second and third cycles, the efficiency drops to 67.08% against 71.66% and 50.67% against 55.01%, respectively. Thus, it is deduced that the programmed 2B sample group's healing efficiency consistently bests those from the non-programmed samples, a consequence of the considerable one-time programming conferred on them since both groups went through similar processes.

A combination of the cooling-induced elongation and entropic relaxation of the molecules during heating as the crystallites melt upon heating serves as the driving force to improve the crack's closing. It is visible from the images shown above that these are primarily macroscopic cracks formed from repeated loading. As such, this mechanism will excellently serve to close inherent microscopic gaps within the material thoroughly. Also, this scheme shows good repeatability with over 50% efficiency achieved after four loading and three healing cycles.

## 3.5.2 FLEXURAL STRESS FOR GROUP 2A & 2B SAMPLES

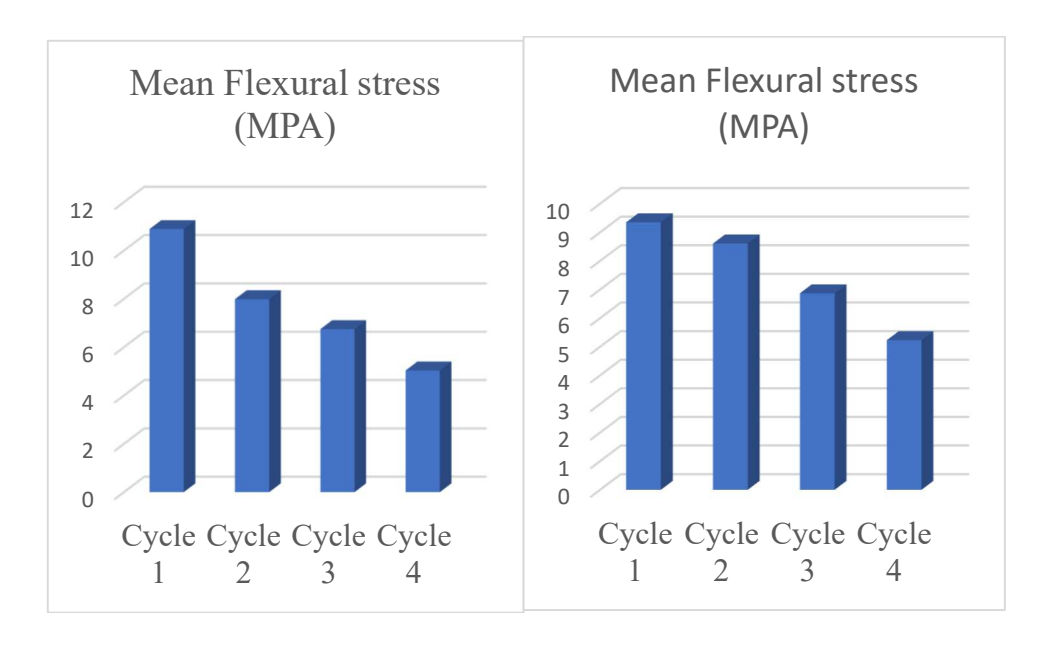
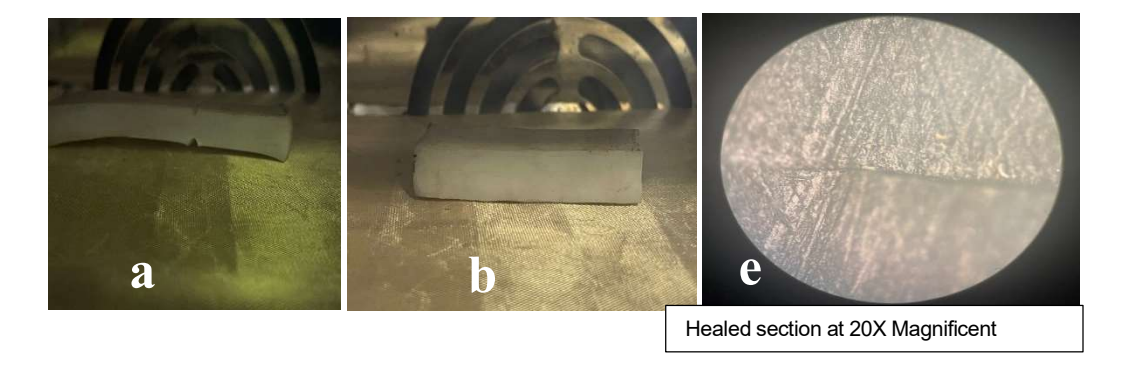


Figure 25-26. Represents the Mean flexural stress of Group 2A & 2B Blends.

This group of samples consists of unprogrammed specimens. Nonetheless, they pass through the same cooling and heating cycles as the Group 2A samples. The three tests showed average flexural stress of 10.89 MPa in the first loading cycle, which dropped to 7.99 MPa in the second, 6.75 MPa in the third, and subsequently, 5.04 MPa fourth loading cycle. During three-point bending testing, the cut section of the material was tested facing downwards, such that the outer facing crack surface was in tension. After that, a clamp with adjustable ends made from aluminum material was used to restrict both longitudinal ends of the specimen while taking care not to compress the material and then placed into the cooling chamber where nitrogen gas was pumped in to cool the enclosure to -45°C. Average flexural stress of 9.35mm was obtained from the three specimens tested during the first loading cycle. By the second, third, and fourth cycles, the flexural stress reduced to 8.61mm, 6.87mm, and 5.23mm, respectively.

## 3.6 Verification of the Close Then Heal Strategy



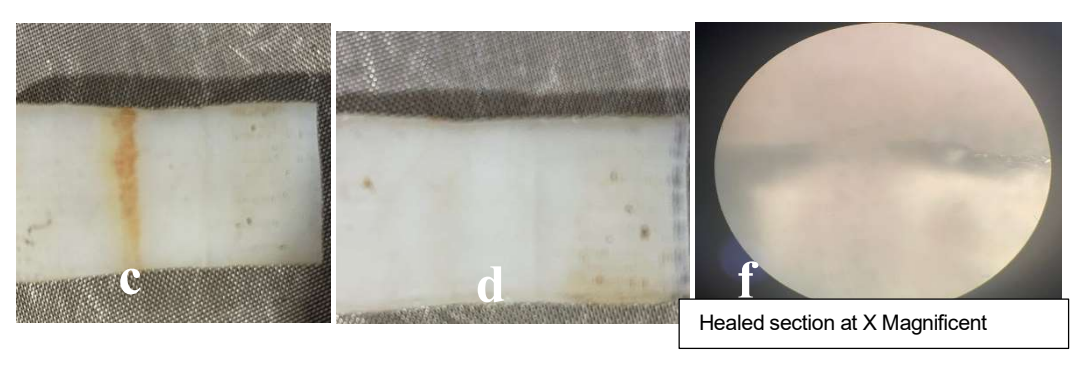


Figure 27a- 32f. Depicts the verification of close then heal method.

A new sample was programmed to 300% strain and tested using a small tensile force of 0.35MPa to hold the specimen in tension to validate the close, then heal strategy as the primary mechanism for narrowing the crack and effectual healing of the material blend. A 1.45mm deep notch made using a knife edge to both sides, results was captured via a microscope. Figure 27a-32f shows the cured specimen with the notch fully closed. The cured specimen once more under the microscope was examined. Compared to the previously observed images, the repaired specimen confirms the healing that has taken place from the combined elongation upon cooling (EUC) and contraction upon heating (CUH).

### 4.0 CONCLUSION

- 1.From the results of characterization, it is evident that proper miscibility was not attained by the processing method used, as evidenced in the double melting peaks of the DSC and the SEM images, as well as mechanical tests. Nonetheless, the blend showed some compatibility between the constituent materials, allowing for some useful application.
- 2.One-way shape memory test showed the 80/20 blend with superior shape memory fixity and recovery ratios with 96.96% and 95.59%, respectively, in the first cycle.
- 3. The polymer blend exhibited a two-way shape memory effect across a temperature window of  $-40^{\circ}$ C and  $100^{\circ}$ C. This combined method of constrained elongation upon cooling and contraction upon heating was repeatable over at least three cycles tested. The 80/20 blend showed better performance with as high as 25.56% EUC in the second cycle.
- 4. A three-point bending test was used to characterize the properties of both 2A and 2B groups, and the maximum load was used to evaluate healing efficiency for the various groups after each cooling and heating cycle.
- 5. Regarding repeatability, the load specimens could carry, flexural stress and healing efficiency all decreased for all groups between the first and fourth cycles.
- 6. The close then-heal strategy using two-way shape memory effect for the blend is very effective for small cracks but not so much for large macroscopic damages.

## 4.1 Acknowledgements

The Authors appreciation goes to the National Science Foundation under award number 1736136 and the Department of Mechanical Engineering @ Southern University Baton Rouge for funding this project.

## **5.0 REFERENCES**

- [1] Wang, Y., Pham, D. T., & Ji, C "Self-healing composites: A review." (Eileen Harkin-Jones, Reviewing Editor). Cog. Eng., vol. 2, no. 1, Aug. 2015, doi: 10.1080/23311916.2015.1075686.
- [2] Blaiszik, B. J., Kramer, S. L. B., Olugebefola, S. C., Moore, J. S., Sottos, N. R., & White, S. R. (2010). Self-Healing Polymers and Composites. Annual Review of Materials Research, 40(1), 179–211. doi:10.1146/annurev-matsci-070909-104532.
- [3] Chen, X., Wudl, F., Mal, A. K., Shen, H., & Nutt, S. R. (2003). New thermally remediable highly cross-linked polymeric materials. Macromolecules, 36(6), 1802-1807.
- [4] Zhong, N., & Post, W. (2015). Self-repair of structural and functional composites with intrinsically self-healing polymer matrices: A review. Composites Part A: Applied Science and Manufacturing, 69, 226-239.
- [5] Zhang, Y., Broekhuis, A. A., & Picchioni, F. (2009). Thermally Self-Healing Polymeric Materials: The Next Step to Recycling Thermoset Polymers? Macromolecules, 42(6), 19061912. https://doi.org/10.1021/ma8027672
- [6] Liu, Y. L., Hsieh, C. Y., & Chen, Y. W. (2006). Thermally reversible cross-linked polyamides and thermo-responsive gels by means of Diels–Alder reaction. Polymer, 47(8), 2581-2586.
- [7] Amamoto, Y., Kamada, J., Otsuka, H., Takahara, A., & Matyjaszewski, K. (2011). Repeatable photoinduced self-healing of covalently cross-linked polymers through reshuffling of trithiocarbonate units. Angewandte Chemie, 123(7), 1698-1701.
- [8] Burnworth, M., Tang, L., Kumpfer, J. R., Duncan, A. J., Beyer, F. L., Fiore, G. L., ... & Weder, C. (2011). Optically healable supramolecular polymers. Nature, 472(7343), 334-337.
- [9] Chuo, T.W.; Wei, T.C.; Liu, Y.L. (2013). Electrically driven self-healing polymers based on reversible guest–host complexation of  $\beta$ -cyclodextrin and ferrocene J Polym Sci, Part A: Polym Chem, 51 (16) (2013), pp. 3395 3403
- [10] Zhang, Z., Hu, Y., Liu, Z., & Guo, T. (2012). Synthesis and evaluation of a moisture-promoted healing copolymer. Polymer, 53(14), 2979-2990.
- [11] Diesendruck, C. E., Sottos, N. R., Moore, J. S., & White, S. R. (2015). Biomimetic self-healing. Angewandte Chemie International Edition, 54(36), 10428-10447.
- [12] Yamaguchi, M., Ono, S., & Terano, M. (2007). Self-repairing property of polymer network with dangling chains. Materials Letters, 61(6), 1396-1399.
- [13] Rahmathullah, M. A. M., & Palmese, G. R. (2009). Crack-healing behavior of epoxy–amine thermosets. Journal of Applied Polymer Science, 113(4), 2191-2201.
- [14] Williams, K. A., Dreyer, D. R., & Bielawski, C. W. (2008). The underlying chemistry of self-healing materials. MRS Bulletin, 33(8), 759-765.
- [15] R. W. Watkin, "Ionic Hydrocarbon Polymers," U.S. Patent 3 264 272, Aug. 2, 1966.